Journal of Power Sources 186 (2009) 532–538

Contents lists available at ScienceDirect

Journal of Power Sources

journal homepage: www.elsevier.com/locate/jpowsour

Silver decorated γ-manganese dioxide nanorods for alkaline battery cathode

Shouyan Wang[a,*], Jining Xie[a], Tierui Zhang[b,1], Vijay K. Varadan[a]

[a] Nanomaterials and Nanotubes Research Laboratory, Center of Excellence for Nano-, Micro-, and Neuro-Electronics, Sensors and Systems, Department of Electrical Engineering, College of Engineering, University of Arkansas, Fayetteville, AR 72701, USA
[b] Department of Chemistry and Biochemistry, University of Arkansas, Fayetteville, AR 72701, USA

ARTICLE INFO

Article history:
Received 15 August 2008
Received in revised form 11 October 2008
Accepted 13 October 2008
Available online 5 November 2008

Keywords:
Manganese dioxide
Hydrothermal
Alkaline battery
Silver nanoparticle
Discharging mechanism

ABSTRACT

γ-Manganese dioxide nanorods were prepared using a simple hydrothermal method based on redox reactions between $S_2O_8^{2-}$ and Mn^{2+} and decoration of silver nanoparticles was performed by a wet impregnation method. The as-prepared materials were characterized by scanning electron microscopy (SEM), transmission electron microscopy (TEM) and X-ray diffraction (XRD). Electrochemical discharging capacity of Ag/MnO_2, MnO_2/multi-walled carbon nanotubes (MWNTs), and Ag/MnO_2/MWNTs electrodes were determined at 0.1 C discharging rate. The results showed that utility efficiency of MnO_2 was greatly enhanced when silver particles were introduced and there was strong interaction between silver nanoparticles and bulk MnO_2 materials. Electrochemical impedance spectroscopy (EIS) measurements were performed to investigate the discharging mechanism of the Ag/MnO_2/MWNTs electrodes. Silver nanoparticles not only enhanced electronic conductivity of the network, but also improved proton diffusion process.

1. Introduction

As a dominant battery for portable electronics, billions of alkaline batteries were consumed annually. One of the battery cathode materials, manganese dioxides, is of technological interest due to their wide use as primary alkaline and secondary lithium-ion batteries, as well as the combination of their structural flexibility with novel chemical and physical properties. Manganese dioxides and their derivatives have also attracted special attentions in many different research areas. Manganese dioxides of particular interests to battery industry are α-, β- and γ-MnO_2, which are built up of [MnO_6] octahedrons (single or double) with shared corners or edges to form channels through the structure. Particularly, γ-MnO_2 has been widely used as cathode active material in primary batteries due to the fact that its electrical potential is reduced slowly compared with the other forms during discharge process.

For a commercial alkaline Zn–MnO_2 battery, its cathode is composed of electrolytic MnO_2 and graphite as electron conductive media, while its anode is made of Zn powder held together by a synthetic gel [1,2]. Although various types of alkaline Zn–MnO_2 primary batteries are available in the market, the electrode utilization efficiency of the active materials, MnO_2 and Zn, still remains low especially under high-drain condition. Furthermore, their storage capacities are largely cathode limited [3]. In order to enhance utilization efficiency of cathode active materials, discharging mechanism of MnO_2 electrodes in alkaline electrolytes has been thoroughly investigated by using different methods, such as nuclear magnetic resonance [4,5], step potential electrochemical spectroscopy (SPECS) [5,6], electrochemical impedance spectroscopy (EIS) [3,7–9], X-ray diffraction (XRD) [10–14], cyclic voltammetry [8,15] and other electrochemical methods [16–19]. Generally, it has been demonstrated that reduction of γ-MnO_2 in an alkaline electrolyte consists of two steps. The first step involves a homogenous proton diffusion process in the lattice of γ-MnO_2, while the second step is a heterogeneous process:

$$MnO_2 + H_2O + e^- \leftrightarrow MnOOH + OH^- \quad (1)$$

$$MnOOH + H_2O + e^- \leftrightarrow Mn(OH)_2 + OH^- \quad (2)$$

Usually, synthesis of γ-MnO_2 for commercial use is performed by an oxidative deposition from Mn^{2+}/H_2SO_4 solutions [4,11,16,20,21]. Nanoscale materials have attracted lots of interests as their intriguing physical and chemical properties are quite different from their bulk counterparts. Size of nanomaterials has also been regarded as a critical process that may bring some novel and unexpected properties. Based on the redox reactions of MnO_4^- and/or Mn^{2+}, γ-MnO_2 nanomaterials have been prepared

* Corresponding author. Current address: Department of Chemistry, University of Michigan, 930 North University Avenue, Ann Arbor, MI 48109, USA. Tel.: +1 734 647 2170; fax: +1 734 647 4865.
E-mail addresses: shouyanw@umich.edu (S. Wang), jxie@uark.edu (J. Xie), tieruiz@ucr.edu (T. Zhang), vjvesm@uark.edu (V.K. Varadan).
[1] Current address: University of California, Department of Chemistry, 501 Big Springs Road, Riverside, CA 92521, USA.

0378-7753/$ – see front matter © 2008 Elsevier B.V. All rights reserved.
doi:10.1016/j.jpowsour.2008.10.086

by several methods, such as chemical deposition process [22,23], hydrothermal [24–31], sol–gel [30], coordination-polymer precursor route [1,32], and hydrothermal treatment of commercial granular γ-MnO_2 crystals [33].

Recently, discharging performance of AA size alkaline batteries with MnO_2 nanowires/nanotubes and graphite as positive active materials and conductive materials, respectively, has been tested [1]. The results showed that utility efficiency of cathode materials can reach up to about 91% at 0.03 C and 85% at about 0.3 C discharging rate. Zhang et al. [23] synthesized a type of mesoporous manganese dioxide by using a template-free self-assembly process at room temperature and electrocatalyst study of as-prepared MnO_2 for air-electrode in a zinc-air battery exhibited better discharge characteristics than that of microsize MnO_2.

Multi-walled carbon nanotubes (MWNTs) have also been demonstrated with a wealth of exceptional structural, mechanical, and electronic properties, which have made them potentially useful for applications in nanotube-reinforced materials [34,35], nanoelectronic devices [36,37], etc. A layer of γ-MnO_2 was adsorbed successfully upon carbon nanotubes (CNTs) surface by using a chemical deposition method [38]. Supercapacitor characteristics of MnO_2/CNTs-based nanocomposite electrodes have also been investigated [20,22,39,40]. A novel air electrode using a combination of dual functional silver/manganese dioxide catalysts based on single-walled carbon nanotubes (SWNTs) was developed by chemically reducing silver permanganate with hydrazine [41]. The electrocatalytical activity was examined. Compared with catalysts supported on mesocarbon microbeads or commercial graphite, higher electrocatalytical activity for oxygen reduction reactions and better discharge performance of zinc-air cell were observed for nano-sized material-based electrodes [42].

Due to their excellent electronic conductivity of silver and MWNTs, combination of these two would be an ideal conductor to form electron-transferring channels during manganese dioxide discharging in alkaline electrolyte. The goal of this work is to improve cathode materials utility efficiency by introducing nano-sized active materials and electron conductors. Interaction between silver nanoparticles and manganese dioxide nanorods and discharging mechanism of γ-MnO_2-based electrodes were also discussed.

2. Experimental

2.1. Materials synthesis and characterization

γ-MnO_2 nanorods were synthesized by a traditional hydrothermal method as reported elsewhere [24]. Manganese sulfate monohydrate (Analytical grade, Alfa Aesar) and a prescribed amount of ammonium persulfate $(NH_4)_2S_2O_8$ (Analytical grade, Sigma–Aldrich) were added into distilled water at room temperature to form a homogeneous solution, which was then transferred into a 40 ml Teflon-lined stainless steel autoclave, sealed and maintained at 90 °C for 12 h. After the reaction was completed, the resulting solid product was filtered, washed with distilled water to remove ion remnant possibly in the final product, and finally dried in air. Silver decorated manganese dioxide nanorods was prepared by a wet impregnation method, which involved an addition of $AgNO_3$ aqueous solution into γ-MnO_2 nanorods suspension under vigorous stirring followed by a drying process. The obtained sample was finally calcined at 200 °C for 0.5 h. Using standard analytical techniques [43], the O/Mn ratio of as prepared MnO_2 and Ag/MnO_2 samples were both determined to be 1.98. Multi-walled carbon nanotubes were derived from a microwave catalytic chemical vapor deposition and a purification process was applied to obtain highly pure carbon nanotubes [44].

A scanning electron microscope (SEM, Philips ESEM XL30) and a transmission electron microscope (TEM, JEOL JEM100CX) were used to investigate the morphology of MnO_2 nanorods. XRD analysis was performed on a Rigaku Miniflex X-ray diffractometer with monochromatized Cu Kα radiation (λ = 1.5406 Å) scanning from 20° to 70°. The Brunauer–Emmett–Teller (BET) surface areas of MnO_2 nanorods and Ag decorated MnO_2 nanorods with carbon nanotubes (Ag/MnO_2/MWNTs) were measured on a surface area and porosimetry system (Micromeritics ASAP2020).

2.2. Electrode assembly and measurement

As-prepared MnO_2 powders were used to make cathode pastes. The weight ratio of active materials to MWNTs is 10:1. A proper amount of 9 M KOH solution was added and mixture was milled by an agate mortar and pestle thoroughly to get the positive paste, followed by pressing onto a 1 cm × 1 cm porous nickel foam. Traditional three-electrode electrochemical cell was assembled for discharging performance measurements. The reference electrode was Hg/HgO and porous nickel foam was used as the counter electrode.

Electrode capacity measurements were performed at a 0.1 C discharging rate (31 mA g^{-1}) at room temperature by using a battery testing system (Arbin instruments, BT4). EIS was measured over frequency range 0.1 Hz to 1 MHz by using a Solartron 1287 electrochemical interface together with a 1255B frequency response analyzer.

3. Results and discussion

3.1. Characteristics of as-prepared MnO_2

The XRD pattern (Fig. 1) confirms the as-synthesized material is mainly γ-MnO_2. For the Ag/MnO_2 sample, its XRD pattern is similar to the precursor indicating a rather uniform distribution of silver particles on MnO_2 supports [45]. All the diffraction peaks can be indexed to an orthorhombic phase of γ-MnO_2 with lattice constants: a = 8.70 Å, b = 2.90 Å, and c = 4.41 Å (Jade, XRD pattern processing software, Materials Data Inc.) which are in good agreement with the standard values (Joint Committee on Powder Diffraction Standards (JCPDS) card no. 65-1298; a = 9.27 Å, b = 2.87 Å, c = 4.53 Å). The peaks at 2θ values of 22.45°, 37.13°, 42.47°,

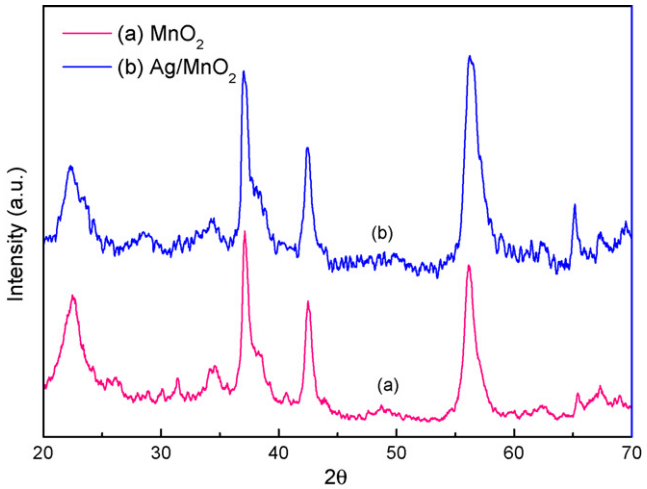

Fig. 1. (a and b) XRD pattern of as-prepared MnO_2 nanorods by a hydrothermal method.

56.26°, and 65.41° correspond to 1 0 1, 2 1 0, 2 1 1, 4 0 2, and 0 2 0 crystal planes of γ-MnO_2, respectively. The small peak at around 28.7° for Ag/MnO_2 sample may be ascribed to β-MnO_2 formed at a relatively high temperature, which is required for the decomposition of silver nitrate. Structure of γ-MnO_2 is widely accepted as a random intergrowth of 1×1 tunnels of pyrolusite and 1×2 tunnels of ramsdellite constructed of [MnO_6] octahedral structures [1,46].

Fig. 2 shows a representative SEM micrograph of as-prepared Ag/MnO_2 powders. It is obvious that synthesized MnO_2 has a rod-like morphology. The EDX spectrum (overall, the aluminum peak comes from the SEM stub used) and mapping (Fig. 3, selected area in Fig. 1) confirmed the homogeneous distribution of silver particles which is consistent with XRD results. The content of silver can also be calculated to be 10.0 wt% by using EDX analysis. It can be seen clearly from a representative TEM image (Fig. 4) that the average size of these nanorods is about 40 nm in diameters and 500 nm in length.

Surface areas of MnO_2 and Ag/MnO_2/MWNTs were measured by BET method. According to the gas adsorption theory in multimolecular layers, the following formula can be applied [47]:

$$\frac{p}{v(p_0 - p)} = \frac{1}{v_m c} + \frac{c-1}{v_m c} \times \frac{p}{p_0} \quad (3)$$

where p and p_0 are the saturation pressure of the gas, v_m is the volume of gas adsorbed when the entire adsorbent surface is covered with a complete unimolecular layer and c is a constant. Fig. 5(a) and (b) are plots of $p/v(p_0 - p)$ vs. p/p_0 for MnO_2 and Ag/MnO_2/MWNTs, respectively. The measured BET surface area for MnO_2 is 35.2 $m^2\,g^{-1}$, while the value is 57.8 $m^2\,g^{-1}$ for Ag/MnO_2/MWNTs. Obviously, the introduction of Ag nanoparticles and carbon nanotubes significantly increases the surface area which is favored for electrochemical reactions occurring during battery discharge.

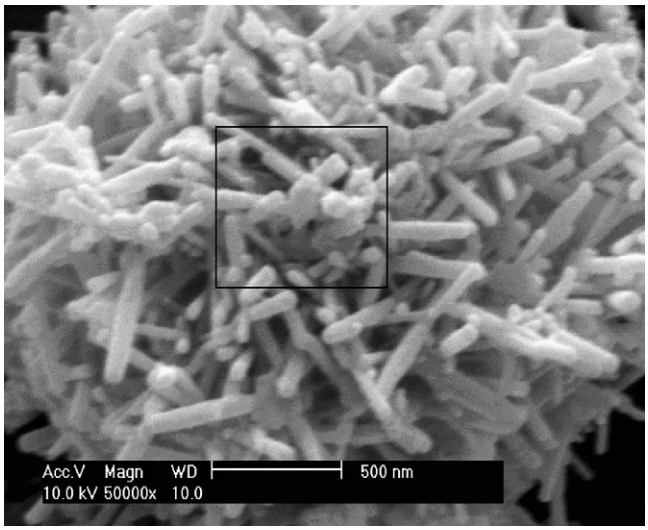

Fig. 2. SEM micrograph of as-prepared Ag/MnO_2 nanorods.

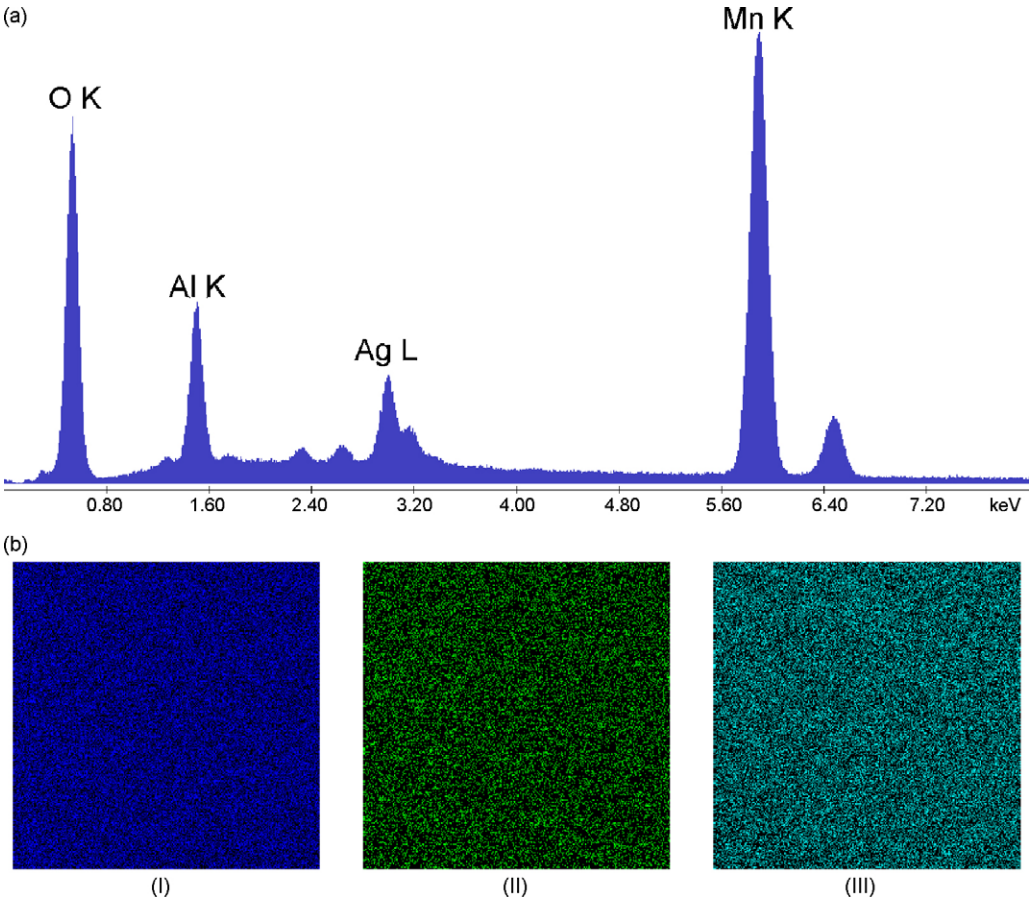

Fig. 3. EDX analysis of as-prepared Ag/MnO_2 nanorods (a) spectrum and (b) elemental mapping (Mn (I), Ag (II) and O (III)).

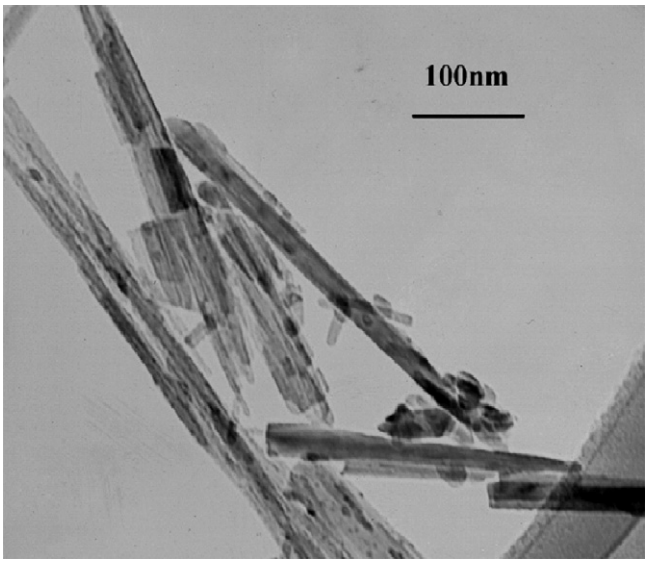

Fig. 4. TEM micrograph of as-prepared Ag/MnO_2 nanorods.

3.2. Discharging performance of the MnO_2 electrodes in alkaline electrolytes

During discharging, the reduction potential of a cathode electrode, described in Eq. (1), is determined by the corresponding

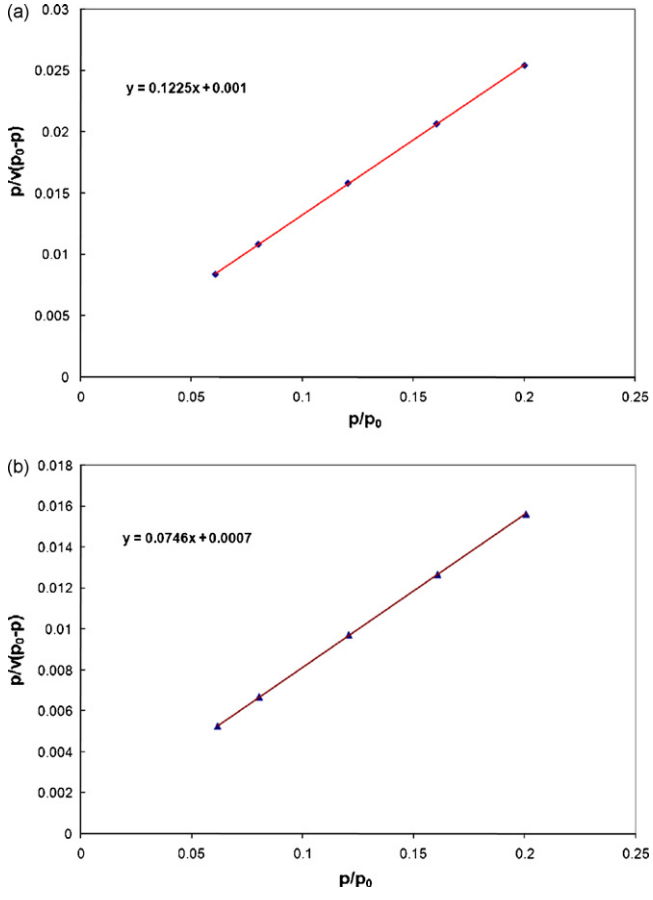

Fig. 5. BET measurements $(p/v(p_0-p)$ vs. $p/p_0)$ for (a) MnO_2 and (b) Ag/MnO_2/MWNTs.

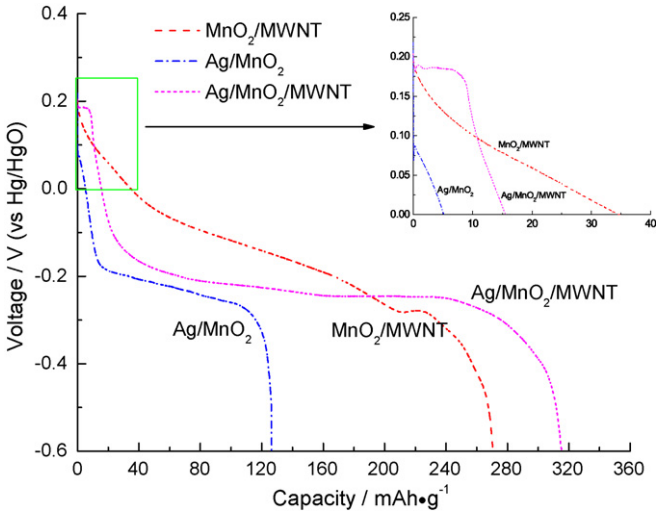

Fig. 6. Discharging curves of the MnO_2 electrodes with different conductors at 0.1 C discharging rate (the inset shows the initial stage of the discharging process).

Nernst equation:

$$E = E^{\circ} + \frac{RT}{F} \ln\left(\frac{[MnO_2] \times [H_2O]}{[MnOOH] \times [OH^-]}\right) \quad (4)$$

where E° is standard reduction potential of MnO_2 electrode and [X] is activity of species X. The other symbols have their usual significances. In our three-electrode electrochemical testing system, the concentration of water and potassium hydroxide can be assumed constant during discharging [6]. Therefore, Eq. (4) may be expressed as following [19,48]:

$$E = E^{\circ\prime} + \frac{RT}{F} \ln\left(\frac{[MnO_2]_{solid}}{[MnOOH]_{solid}}\right) \quad (5)$$

where $E^{\circ\prime}$ takes into consideration the contributions to the potential from $[H_2O]$ and $[OH^-]$, $[X]_{solid}$ is mole fraction of MnO_2 and MnOOH species in solid phase and $[MnO_2]_{solid} + [MnOOH]_{solid} = 1$. The discharging potential of MnO_2 electrode in alkaline electrolytes can be calculated at various stages of discharge according to Eq. (5).

Fig. 6 shows typical discharging curves of MnO_2-based electrodes with different electrode components. The open circuit voltages (OCV) for MnO_2/MWNT, Ag/MnO_2 and Ag/MnO_2/MWNT were measured to be 0.209, 0.206 and 0.207 V, respectively. Usually, we can predict an OCV increase with a higher Mn^{4+} content and a higher relative proportion of less stable MnO_2 phases; i.e., ramsdellite and cation vacancies [21]. It is also generally believed that drying at 150 °C or above will cause a loss of cation vacancy protons along with an equivalent amount of oxygen, from the electrolytic manganese dioxide (EMD) lattice [31] and thus a loss of high voltage and reduced electrochemical performance [4]. Here, all electrodes show almost same higher OCV comparable to commercial EMD although Ag/MnO_2 was calcined to decompose silver nitrate at relatively high temperature. This may be ascribed to the relatively short heating treatment period (half an hour here vs. several hours in literatures) and most of the protons are still keep intact after heating treatment.

The potential of the MnO_2/MWNTs electrodes decreases gradually with discharge duration in alkaline solution as defined by Eq. (5), which implies that discharging of manganese dioxide is a homogeneous process [19]. When a manganese dioxide is discharged, MnOOH is produced as a primary product on the surface of bulk MnO_2 particles, and the proton and ionic diffusion process has been considered as the rate-determining step in overall discharge reactions [1,4–6,9–13,16–19]. The potential decrease of the

manganese dioxide electrodes during discharge is caused by accumulation of MnOOH, which can be interpreted by a concept of solid phase diffusion of MnOOH. The diffusion process does not need to be considered as the actual movement of Mn and O atoms and its effect can be attained by diffusion of protons and electrons only [1,6,9,19]. By diffusion, the concentration of MnOOH at the electrode surface decreases after current stops, but since it is merely a leveling of MnOOH concentration in solid phase, some accumulations of MnOOH at the electrode is inevitable. Consequently, decrease in potential takes place. The first discharging step occurs between 0.3 and −0.4 V (vs. Hg/HgO, the same as below) and the second step starts at about −0.4 V. In most cases, except for those at very low-discharge current densities, γ-MnO_2 is rarely discharged to the heterogeneous step. The abovementioned second discharge step represents only a minor contribution to the total discharge capacity of a practical battery [12,19].

It also can be seen from Fig. 6 that silver particles have great effects on the discharging performance of MnO_2. About 257 mAh g^{-1} of discharge capacity was achieved for the typical MnO_2/MWNTs electrode, while capacity increased greatly to about 302 mAh g^{-1} for the silver decorated MnO_2 electrode at −0.4 V (vs. Hg/HgO) cutoff potential for both. For silver decorated MnO_2 electrode without MWNTs conductive media, the capacity is about 124 mAh g^{-1} only which can be ascribed to the poor connecting network for electron transfer. In this case, there are only silver particles, which are dispersed finely on the surface of bulk MnO_2 nanorods surface, serving as electron conveying agent. Most importantly, as all electrodes has an OCV around 1.59 V vs. zinc, the energies calculated are 242, 278 and 102 mWh g^{-1} for MnO_2/MWNTs, Ag/MnO_2/MWNTs and Ag/MnO_2 with 1.1 V vs. zinc cutoff potential, respectively. Detailed discharging mechanism is discussed in the following section.

3.3. Discharging mechanism of the silver decorated MnO_2 electrodes

It is interesting to study the underlying mechanism behind superior discharge performance of silver decorated γ-MnO_2 in this work compared with other chemical manganese dioxides. In alkaline solution, concentration of H^+ ion is so low that the possibility of the disproportionation reaction (that is, $2MnOOH + 2H^+ \rightarrow MnO_2 + Mn^{2+} + 2H_2O$) is very small [11]. Therefore, the removal of MnOOH is performed by solid phase diffusion only as discussed before. Cheng et al. [1] studied discharging performance of γ-MnO_2 nanowires/nanotubes with graphite as the conductive material and their results showed that employment of γ-MnO_2 nanowires/nanotubes played a significant role in improved performance of AA size batteries. Since the surface area is high for nanoscale crystalline γ-MnO_2, sufficient material contact within electrode was resulted, thereby favoring diffusion process [1]. Furthermore, nanosize conducting MWNTs can be distributed uniformly and form an efficient electron transferring matrix throughout the electrode. As the result, a low-internal resistance and high-electrical conductivity were observed for the testing cell [22,49].

During initial discharging stage as shown in the inset of Fig. 6, the potential of the Ag/MnO_2/MWNTs electrode is constant indicating that silver is partly oxidized during the synthesis of active materials. The potential is consistent with the discharging potential of Ag_2O/Ag couple (about 0.2 V) in alkaline electrolytes. And the weight percentage of silver oxide, about 40%, expressed as amount of silver oxide relative to the total amount of silver and silver oxide together, can be calculated according to the electrode discharging capacity during that period. As a matter of fact, the utility efficiency of the Ag/MnO_2/MWNTs electrodes can reach as high as 95% at 0.1 C discharging rate with a −0.4 V cutoff potential subtracting the contribution of Ag_2O/Ag couple. There are only slight potential variations for the Ag/MnO_2 electrodes since the polarization for this electrode is too high as we mentioned above. As water is a reactant in this expression, its availability is crucial for high-rate discharge. It is likely that high-surface area active materials benefit from rapid exchange of water from one cell region to another and thus enhanced their electrode performances [1].

According to SPECS results [5,6], the reduction process of MnO_2 to form MnOOH actually occurs via several homogeneous steps during discharge in alkaline electrolytes (9 M KOH) as shown in following:

Step 1. Reduction of Mn^{4+} on or close to surface of the MnO_2 particles (0–0.1 V).
Step 2. Reduction of ramsdellite domains (−0.1 V).
Step 3. Reduction of pyrolusite domains (−0.2 V).

The potential of the Ag/MnO_2/MWNTs electrodes, unlike the MnO_2/MWNTs electrodes, decreased sharply to about −0.2 V (directly to the third step after a short discharging period as shown in Fig. 6) and then kept roughly constant. The only difference between these two electrodes, the Ag/MnO_2/MWNTs and the MnO_2/MWNTs, is their composition. Hence, silver nanoparticles are believed to play significant roles for improved battery performances.

Introducing silver nanoparticles to MnO_2 produces a strong Ag–MnO_2 interaction [45] and their surface structure significantly determines the intensity of interaction. H_2O, which is an abundant source of protons during discharging, may decompose at the solid–solution interface, and protons are introduced into the lattice forming OH^- [19]. Silver nanoparticles mounted on the surface of MnO_2 nanorods can not only decrease the resistance of the electrodes but also promote the surface proton diffusion process [50]. On or close to the nanorods surface, MnO_2 is reduced to MnOOH dramatically owing to silver nanoparticles. Especially, near the newborn surfaces of silver, the primary discharging products accumulate rapidly due to the relatively slow removal of MnOOH [18,19]. Thus the electrode potential decreases quickly to the third step according to Nernst equation till a new proton and electron diffusion equilibrium is established.

A porous electrode that involves Faraday charge transfer can be represented as a transmission line equivalent circuit [9,51,52]. Two types of currents through the interface of electrode should be distinguished, which are the current due to proton insertion and electron migration between MnO_2 particles (that is Faraday current), and the non-Faraday current to a charge/discharge double layer. The Faraday branch may be represented by a charge transfer resistance R_{ct} and by a Warburg impedance W, while the non-Faraday displacement current branch may be represented by a distributed double-layer capacitor, constant phase element (CPE). The distributed capacitance and resistance are used to represent the energy dissipation in a porous electrode. The Warburg impedance occurs when the charge carriers diffuse through a material. R_{ct} is believed to relate not only to the surface condition of γ-MnO_2 particles, but also to the water activity in vicinity of MnO_2 particles [9]. High values of R_{ct} will result in high-electrochemical over-potentials during discharge. R_{ct} can also be used to evaluate the quality of γ-MnO_2 and its value may vary substantially with different γ-MnO_2 [9].

EIS was conducted to further understand the reaction processes of the MnO_2 electrodes. It can be seen from Fig. 7(a) and its inset that the typical Ag/MnO_2/MWNTs electrode shows the lowest reaction resistance. Usually, equivalent circuit, shown in Fig. 7(b), is selected to represent a porous electrode matrix for ion diffusion

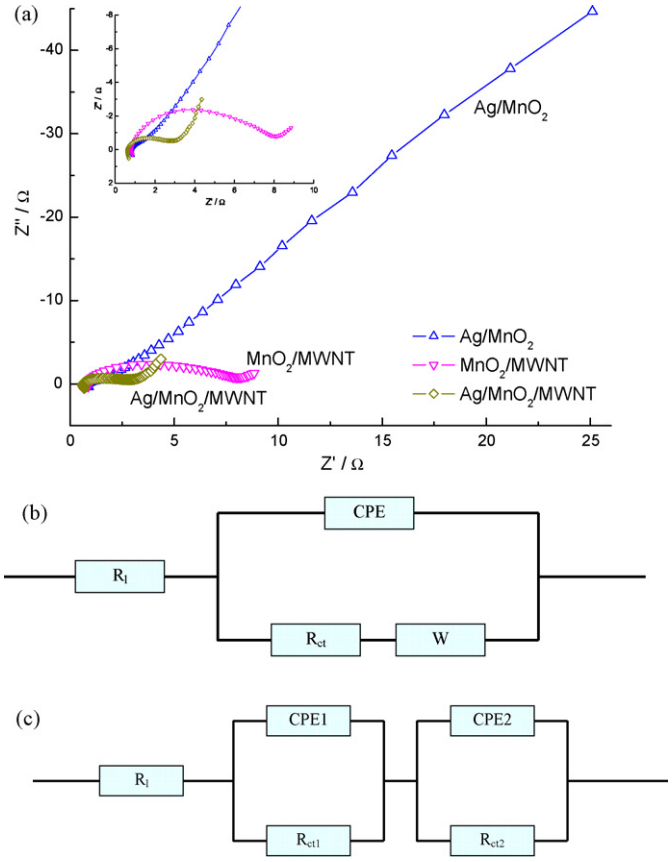

Fig. 7. EIS curves for different MnO_2 electrodes (a) at an open-circuit potential and the equivalent circuit models used in the impedance fitting for the electrodes (b) without and (c) with silver decoration.

with local proton intercalation into the lattice of MnO_2 without silver decoration [8,9,51,52], where R_l is the alkaline solution ohmic resistance. Since nano-silver particles were dispersed evenly throughout the bulk MnO_2 surface, the newborn silver particle with high-electro-catalytic abilities and low resistances accelerate the proton and electron diffusion throughout the electrode. For the Ag/MnO_2/MWNTs electrodes, two electrochemical reactions should take place. The first one is ascribed to reduction of silver oxide, which is consistent with a constant potential observed in Fig. 6 during initial discharging stage. And the second one was reduction of MnO_2 active materials—proton diffusion through the lattice of MnO_2 without a Warburg impedance (Fig. 7(c)).

Simulation results (ZSimpWin 3.10, EChem Software) of EIS curves for all electrodes studied in this work are listed in Table 1. It is indicated that MWNTs improve the electrode conductivity dramatically. The reaction resistance drops from 108.8 and 96.9 to 2.5 and 5.7 $\Omega\,cm^2$ for the Ag/MnO_2 and the Ag/MnO_2/MWNTs electrodes, respectively. The MnO_2 reduction resistance of the Ag/MnO_2/MWNTs electrodes also decreases slightly compared with the MnO_2/MWNTs electrodes (from 6.9 to 5.7 $\Omega\,cm^2$), which may be attributed to the electro-catalysis of silver nanoparticles. Most importantly, no Warburg resistance was detected in either silver contained electrode suggesting an obvious different discharging process as expected. The higher electronic conductivity of and improved proton diffusion by silver nanoparticles results in higher discharging capacities of the Ag/MnO_2/MWNTs electrodes.

Table 1
Equilibrium circuit parameters of different MnO_2 electrodes.

	$R_l/\Omega\,cm^2$	$R_{ct1}/\Omega\,cm^2$	$R_{ct2}/\Omega\,cm^2$	$W/S\,s^{0.5}\,cm^{-2}$
MnO_2/MWNTs	0.78	–	6.9	0.58
Ag/MnO_2	0.75	108.8	96.9	–
Ag/MnO_2/MWNTs	0.57	2.5	5.7	–

4. Conclusion

γ-Manganese dioxide nanorods were synthesized by a hydrothermal method. The diameter of the as-obtained nanorods is about 40 nm, with a length of 500 nm. Silver nanoparticles, decorated on the surface of the nanorods evenly by a wet impregnation method, have greatly interacted with MnO_2 during discharging in alkaline electrolytes. Capacities of as-prepared electrodes were measured and the material utility efficiency can reach up to about 95% for silver decorated MnO_2 with MWNTs conductive media at 0.1 C discharging rate. The potential of the Ag/MnO_2/MWNTs electrodes is almost constant during discharge. Discharging mechanism studies showed that silver nanoparticles not only accelerate the electron conducting but also improve the proton diffusion throughout the electrode, which is consistent with the results of the EIS measurements.

Acknowledgements

The authors would like to thank Professor Z. Ryan Tian for valuable discussions. And Arkansas Analytical Lab (AAL) is acknowledged for the access of the SEM equipment.

References

[1] F.Y. Cheng, J. Chen, X.L. Gou, P.W. Shen, Adv. Mater. 17 (2005) 2753–2756.
[2] C.C. Yang, S.J. Lin, J. Power Sources 112 (2002) 174–183.
[3] S. Rodrigues, N. Munichandraiah, A.K. Shukla, J. Appl. Electrochem. 30 (2000) 371–377.
[4] Y. Paik, W. Bowden, T. Richards, C.P. Grey, J. Electrochem. Soc. 152 (2005) A1539–A1547.
[5] Y. Paik, W. Bowden, T. Richards, R. Sirotina, C.P. Grey, J. Electrochem. Soc. 151 (2004) A998–A1011.
[6] G.J. Browning, S.W. Donne, J. Appl. Electrochem. 35 (2005) 871–878.
[7] K. Tachibana, K. Matsuki, J. Power Sources 74 (1998) 29–33.
[8] M. Ghaemi, L. Khosravi-Fard, J. Neshati, J. Power Sources 141 (2005) 340–350.
[9] D.Y. Qu, Electrochim. Acta 48 (2003) 1675–1684.
[10] W.C. Maskell, J.A.E. Shaw, F.L. Tye, J. Appl. Electrochem. 12 (1982) 101–108.
[11] A. Era, Z. Takehara, S. Yoshizaw, Electrochim. Acta 13 (1968) 207–213.
[12] R. Patrice, B. Gerand, J.B. Leriche, L. Seguin, E. Wang, R. Moses, K. Brandt, J.M. Tarascon, J. Electrochem. Soc. 148 (2001) A448–A455.
[13] G.S. Bell, R. Huber, Electrochim. Acta 10 (1965) 509–512.
[14] K.M. Parida, S.B. Kanungo, B.R. Sant, Electrochim. Acta 26 (1981) 435–443.
[15] V.K. Nartey, L. Binder, A. Huber, J. Power Sources 87 (2000) 205–211.
[16] G.J. Browning, S.W. Donne, J. Appl. Electrochem. 35 (2005) 437–443.
[17] S.B. Kanungo, K.M. Parida, B.R. Sant, Electrochim. Acta 26 (1981) 1147–1156.
[18] A. Era, Z. Takehara, S. Yoshizawa, Electrochim. Acta 12 (1967) 1199–1212.
[19] A. Kozawa, R.A. Powers, J. Electrochem. Soc. 113 (1966) 870–878.
[20] Y.K. Zhou, B.L. He, F.B. Zhang, H.L. Li, J. Solid-State Electrochem. 8 (2004) 482–487.
[21] M. Devenney, S.W. Donne, S. Gorer, J. Appl. Electrochem. 34 (2004) 643–651.
[22] V. Subramanian, H. Zhu, B. Wei, Electrochem. Commun. 8 (2006) 827–832.
[23] G.Q. Zhang, X.G. Zhang, H.L. Li, J. Solid-State Electrochem. 10 (2006) 995–1001.
[24] X. Wang, Y.D. Li, Chem.-Eur. J. 9 (2003) 300–306.
[25] X. Wang, Y. Li, J. Am. Chem. Soc. 124 (2002) 2880–2881.
[26] L.I. Hill, R. Portal, A. Verbaere, D. Guyomard, Electrochem. Solid-State Lett. 4 (2001) A180–A183.
[27] L.I. Hill, A. Verbaere, D. Guyomard, J. Electrochem. Soc. 150 (2003) D135–D148.
[28] F.Y. Cheng, J.Z. Zhao, W. Song, C.S. Li, H. Ma, J. Chen, P.W. Shen, Inorg. Chem. 45 (2006) 2038–2044.
[29] W.N. Li, J.K. Yuan, X.F. Shen, S. Gomez-Mower, L.P. Xu, S. Sithambaram, M. Aindow, S.L. Suib, Adv. Funct. Mater. 16 (2006) 1247–1253.
[30] S. Bach, M. Henry, N. Baffier, J. Livage, J. Solid-State Chem. 88 (1990) 325–333.
[31] S.M. Davis, W.L. Bowden, T.C. Richards, J. Power Sources 139 (2005) 342–350.
[32] Y.J. Xiong, Y. Xie, Z.Q. Li, C.Z. Wu, Chem.-Eur. J. 9 (2003) 1645–1651.
[33] Z.Y. Yuan, Z.L. Zhang, G.H. Du, T.Z. Ren, B.L. Su, Chem. Phys. Lett. 378 (2003) 349–353.
[34] A. Peigney, Nat. Mater. 2 (2003) 15–16.
[35] H.M. Hseuh, N.H. Tai, T.P. Perng, S.D. Chyou, Key Eng. Mater. 249 (2003) 65–68.

[36] A.M. Fennimore, T.D. Yuzvinsky, W.Q. Han, M.S. Fuhrer, J. Cumings, A. Zettl, Nature 424 (2003) 408–410.
[37] K. Sivakumar, B. Panchapakesan, J. Nanosci. Nanotechnol. 5 (2005) 313–318.
[38] X.P. Huang, C.X. Pan, X.T. Huang, Mater. Lett. 61 (2007) 934–936.
[39] E. Raymundo-Pinero, V. Khomenko, E. Frackowiak, F. Beguin, J. Electrochem. Soc. 152 (2005) A229–A235.
[40] C.Y. Lee, H.M. Tsai, H.J. Chuang, S.Y. Li, P. Lin, T.Y. Tseng, J. Electrochem. Soc. 152 (2005) A716–A720.
[41] G.Q. Zhang, X.G. Zhang, Y.G. Wang, Carbon 42 (2004) 3097–3102.
[42] D. Zhang, T. Sotomura, T. Ohsaka, Chem. Lett. 35 (2006) 520–521.
[43] D. Glover, J.B. Schumm, A. Kozawa, Handbook of Manganese Dioxides Battery Grade, IBA Inc., USA, 1989, pp. 22–45.
[44] V.K. Varadan, J.N. Xie, Smart Mater. Struct. 11 (2002) 728–734.
[45] R. Xu, X. Wang, D.S. Wang, K.B. Zhou, Y.D. Li, J. Catal. 237 (2006) 426–430.
[46] A.M. Bystrom, Acta Chem. Scand. 3 (1949) 163–173.
[47] S. Brunauer, P.H. Emmett, E. Teller, J. Am. Chem. Soc. 60 (1938) 309–319.
[48] A. Kozawa, J.F. Yeager, J. Electrochem. Soc. 112 (1965) 959–963.
[49] Y.T. Wu, C.C. Hu, J. Electrochem. Soc. 151 (2004) A2060–A2066.
[50] J.M. Vohs, B.A. Carney, M.A. Barteau, J. Am. Chem. Soc. 107 (1985) 7841–7848.
[51] D.Y. Qu, J. Power Sources 156 (2006) 692–699.
[52] D.Y. Qu, Electrochim. Acta 49 (2004) 657–665.